DOI: 10.1021/ma101121f

Macromolecules
ARTICLE

Transition Moment Orientation Analysis on a Smectic C Liquid Crystalline Elastomer film

Wilhelm Kossack,[†] Periklis Papadopoulos,*[,†] Patrick Heinze,[‡] Heino Finkelmann,[‡] and Friedrich Kremer[†]

[†]*Institut für Experimentelle Physik I, Universität Leipzig, 04103 Leipzig, Germany, and*
[‡]*Institut für Makromolekulare Chemie, Albert-Ludwigs-Universität Freiburg, 79104 Freiburg, Germany*

Received May 20, 2010; Revised Manuscript Received August 6, 2010

ABSTRACT: A novel spectroscopic approach is presented, which reveals a complete characterization of the quadratic averaged orientation of infrared transition dipole moments in any IR-translucent material. Transmission spectra of the samples are acquired as a function of polarization Φ and inclination θ, so that the electric field in the sample can be varied in all three dimensions. Based on Maxwell's equations and the quantum mechanic transition probabilities, a connection between optical and molecular properties is derived, that enables one to obtain the three-dimensional molecular order matrix or, alternatively, the scalar order parameter and biaxiality. Since the method takes advantage of the specificity of the IR spectral range the initial orientation distribution as well as its response to external excitation can be traced in detail for each molecular moiety. As an example, the results on a smectic liquid crystal elastomer (LCE) under shear are presented. The analysis of different absorption bands of the LCE film in the near-infrared region proves the consistency and versatility of the approach.

Introduction

The biaxiality of molecular orientation in condensed matter is reflected in macroscopic properties, such as optical, mechanical, and electrical. In particular, organic systems based on macromolecules may exhibit a hierarchical molecular structure over multiple length scales. For all these cases, a technique that can study the three-dimensional anisotropy on the molecular level and its response to external fields is desirable.

Biaxial molecular anisotropy can be measured by NMR quadrupole splitting,[1,2] but this approach requires incorporation of deuterium at special sites. The measurements are performed in high magnetic fields and are difficult to combine with other techniques, such as mechanical measurements. Optical techniques based on reflection measurements (spectroscopic ellipsometry) are in general limited to thin films and rely on the applicability of analytical models in order to provide the absorption coefficient anisotropy.[3] In addition, poorly prepared samples may give rise to unacceptable artifacts. In general, ellipsometry can measure accurately the anisotropy of the real part of the refractive index, or, equivalently, the dielectric function, but not the much lower absorption coefficient that is found in organic materials. The latter is, however, more important, because it can be related to the molecular structure in a straightforward way. Measurements in transmission geometry can more easily provide information concerning the molecular orientation (e.g., liquid crystals);[4]; thus, it enables one to quantify the orientation distribution of different molecular groups.[5,6] Polarized IR spectroscopy (for a review see Griffiths and Haseth[7]) is commonly applied using several assumptions, most importantly the rotational symmetry of the orientation distribution with respect to its main axis lying on the sample plane, that allows to limit the variation of the electric field in the sample plane only.

*To whom correspondence should be addressed. E-mail: papadopoulos@physik.uni-leipzig.de.

In the case of biaxial samples it is imperative that the electric field components in all three dimensions are varied. IR[8−10] as well as Raman[11] polarization dependent spectroscopic studies have been performed to analyze arbitrary molecule orientation distributions. In these cases polarized light at non-normal incidence is used, probing the transition moments normal to the sample plane. The present publication shares this principle; to the best of the authors' knowledge it is the first approach strictly based on Maxwell's equations, which collects more than 100 non-normal incident spectra and treats them in a closed form together with the data at normal incidence resulting in an overdetermined system. Because of the varying inclination, anisotropic reflection and birefringence[12] have to be considered in conjunction with the biaxial properties of the sample (for a detailed treatment see Yeh[13] or Orfanidis[14]). Thus, no assumptions about symmetry are necessary. Working in transmission mode has the advantage that sample preparation is not critical. The technique can be applied even to samples much thicker than the wavelength, provided that the absorbance remains low enough.

As an example we present measurements on the order of the molecular moieties of a liquid crystalline elastomer (LCE, a review is given by Warner and Terentjev[15]). These polymeric systems combine the molecular order of liquid crystals with the entropy-controlled mechanical properties of amorphous cross-linked polymer networks, using a multiple-step synthetic procedure.[16−18] The network conformation is, thus, strongly dependent on the molecular orientation and anisotropy of the liquid crystal mesogens, giving rise to strong anisotropy of the (electro)mechanical properties. The system in this study is a main-chain LCE exhibiting a smectic C mesophase over a broad temperature range. Since their layer normal is not parallel to the nematic director,[19,20] orienation of the director alone may yield a biaxial monodomain or centrosymmetric polydomain morphology, depending on the synthetic route and postprocessing. In the latter case, the anisotropy effects are averaged out at a macroscopic scale. Consequently, controlling the inner architecture enables one to induce special properties to

 Published on Web 08/19/2010

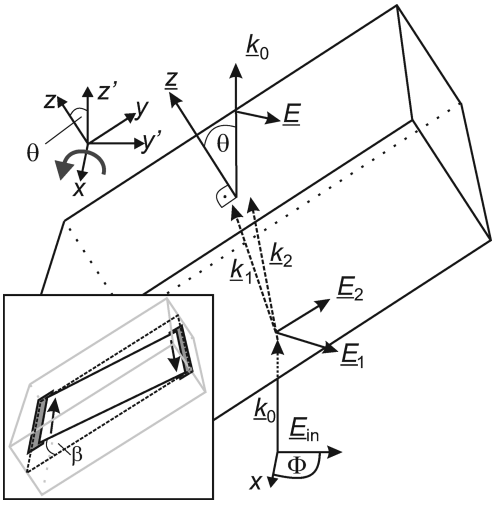

Figure 1. Sketch of the sample with wave vectors $\underline{k}$ and electric fields $\underline{E}$. The vectors indexed with $_{1,2}$ describe the wave inside the medium, the incident ($\underline{k}_0$, $\underline{E}_{in}$) and transmitted wave ($\underline{k}_0$, $\underline{E}$) are shown as well. The rotation of sample and holder is performed with respect to the x axis (gray arrow) of the sample frame (unprimed coordinate system), which is identical with the x' axis of the laboratory frame (primed system). Therefore, the film surface normal is always the z axis and the inclination angle is θ. The angle between the electric polarization and the x axis is denoted as Φ. The inset depicts the shear deformation (shear angle β) and the sample holder (dark gray) in the same reference frame.

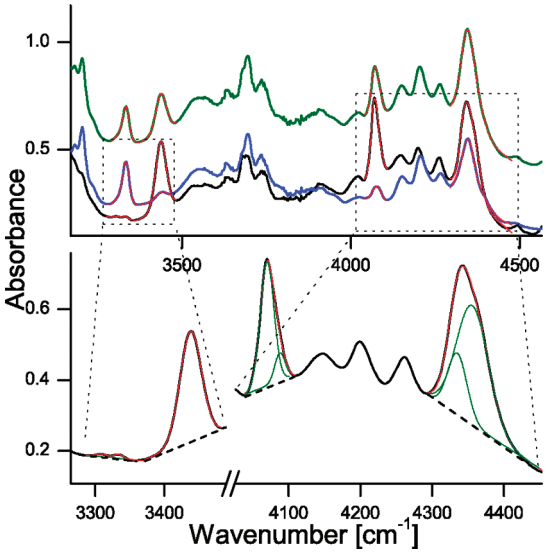

Figure 2. Absorption spectra of a smectic LCE film taken for different combinations of θ and Φ with fitted absorption profiles (red), The black line corresponds to $\underline{E} \| x$ ($\Phi = 0°$, $\theta = 0°$), the blue line to $\underline{E} \| y$ ($\Phi = 90°$, $\theta = 0°$) and the green one lies in the $y-z$ plane ($\Phi = 90°$, $\theta = -60°$). The lower plot is an enlargement with the subtracted baselines (dashed) and deconvolved Gaussian profiles (green).

these materials. Recent theoretical studies predict a domain alignment of polydomain smectic C LCEs if shear perpendicular to the nematic director is applied.[21,22] Polarization-dependent IR absorption measurements in two dimensions under the influence of mechanical fields have been carried out on similar systems before.[23−25] In this study, the orientation, molecular order, and biaxiality of different mesogen parts are analyzed with respect to shear angle in an attempt to characterize the coupling of the liquid crystal director to the elastomer network.

Experimental Section

Measurement Setup. To study the three-dimensional molecular order of a polymer film a Bio-Rad FTS 6000 FTIR-spectrometer is provided with a custom-made tilting apparatus containing the sample holder, that enables one to rotate the sample about a horizontal axis (x axis in Figure 1) perpendicular to the propagation direction of light (z'). Consequently, a parallel incident beam has to be used instead of a focused one to avoid the conic distribution of the wave vector. Therefore, one can choose an arbitrary combination of inclination and polarization angle by the use of a wire grid polarizer and, hence, select a special combination of electric field and wave vector.

To separate the spatial contributions of the absorption ellipsoid and improve fitting by overdetermining the equation system, the tilt or inclination angle of the sample θ is varied between -60 and $+60°$ in steps of 10°, while the polarization angle Φ, measured from the x axis, varies between 0° and 180° in steps of 18°, determining the electric field ($\underline{E}$) and the wave vector ($\underline{k}$) of the incident light. In contrast to usual measurements, the fingerprint region is not chosen, because of the high absorbance due to the large number of bands in this region and the thickness of the sample. For each combination of θ and Φ one IR spectrum in the range of [3000, 6000] cm^{-1} is acquired with a spectral resolution of 4 cm^{-1} using a photoconductive InSb detector. Three spectra collected for different polarization and inclination angles are shown in Figure 2 to illustrate the dependence of the absorbance on θ and Φ.

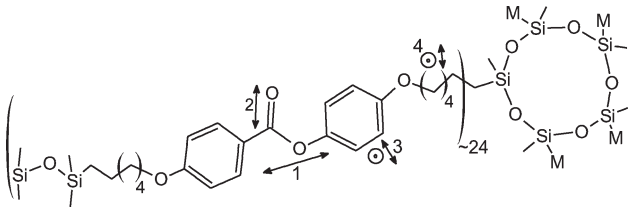

Figure 3. Chemical structure of the monomer and the cross-linker $(SiOCH_3)_5$, building the macromolecule. M denotes positions of other monomer chains, and the arrows show the orientation of the transition dipole moments (Table 1).

The film length corresponding to the distance of the two edges of the holder is 6 mm (see Figure 1) and the width 8.8 mm. The thickness of the sample $d = 450$ μm is measured with a capacitive displacement transducer (Mitutoyo, Digimatic Indicator) with a tolerance of ~15 μm. Furthermore, shear is applied to the samples by movable metal plates on which the sample is fixed in the preferred direction using a solvent-free glue (Figure 1). The positions of the plates are controlled with a micrometer screw, while the retracting force response can be measured by a collinearly mounted force sensor (burster GmbH).

Samples. The liquid crystalline elastomer (LCE) analyzed in this study is a free-standing smectic C main chain elastomer film, synthesized in a two step cross-linking procedure,[26,27] following the route described by Donnio et al.,[16] which is an advancement of Küpfer and Finkelmann.[28] The chemical structure including stoichiometry is shown in Figure 3. The measured transition moments are indicated as well (see Table 1).

Theoretical Part

Propagation of Electromagnetic Waves. The current work is concerned with the propagation of electromagnetic waves through a biaxial lossy medium with arbitrarily oriented principal axes of the absorption ellipsoid. Since the intensity transmitted through the sample is measured, the theoretical background, that governs the propagation of light in anisotropic dielectric and nonmagnetic media, is provided first. The transmitted intensity depends on the electromagnetic

Table 1. Assignment of Absorption Bands

index	wavenumber $\bar{\nu}$ (cm^{-1})	assignment	orientation with respect to the director
1	3334	combination band of the ester C=O stretching vibration and a stretching vibration of the phenyl[29] superimposed by a weak band at ~3310 cm^{-1}	∥
2	3438	first overtone of carbonyl group stretching[30]	⊥
3	4068	combination band of the aromatic CH stretching vibration (3080 cm^{-1}) and CH deformation vibration (1037 cm^{-1})[31,32]	⊥
4	4360	two combination bands consisting of the CH_2 stretching vibrations (antisymmetric 2925 cm^{-1} and symmetric 2870 cm^{-1}) and a CH_2 scissoring vibration (1465 cm^{-1})[33]	⊥

wave (namely its polarization, wavelength and intensity) as well as on the properties of the medium (indicatrix and thickness). Naturally, the relative orientation of the two also plays an important role; here, this is treated in terms of the wave vectors and the film plane surface normal (compare Figure 1).

The propagation equation for electromagnetic waves inside an anisotropic dielectric medium (that can be derived directly from Maxwell's equations[13]) is given, where $\boldsymbol{n}$ is the indicatrix, c_0 the speed of light in vacuum, $\underline{k}$ is the wave vector, ω the frequency and $\underline{E}$ the electric field of the wave.

$$\underline{k} \times (\underline{k} \times \underline{E}) + \frac{\omega^2}{c_0^2} \boldsymbol{n}^2 \cdot \underline{E} = 0 \qquad (1)$$

The boundary conditions lead to the following continuity condition (Snell's law) in terms of the wave vectors, $\underline{k}$; the effective refractive index, n; the reference frame of the sample, y; and the angle between the surface normal (z) and the wave vector, θ (the refractive index of the surrounding medium is set to 1, for definitions see Figure 1).

$$\underline{k}_0 y = \sin\theta = n_m \sin\theta_m = \underline{k}_m y \qquad (2)$$

where the $_{m(0)}$-indexed values correspond to the quantities inside (outside) the medium. Combining eq 1 and eq 2 enables one to find the allowed propagation directions ($\underline{k} = \underline{k}_m$) inside medium and the corresponding electric fields.[12−14] Equation 1 can thus be written as

$$\left\{ \begin{pmatrix} -k_{0,y}{}^2 & 0 & 0 \\ 0 & -k_{0,y}{}^2 - k_z{}^2 & k_{0,y} k_z \\ 0 & k_{0,y} k_z & -k_{0,y}{}^2 \end{pmatrix} + \frac{\omega^2}{c_0{}^2} \boldsymbol{n}^2 \right\} \underline{E} = 0 \qquad (3)$$

By setting the determinant of the resulting matrix in eq 3 to zero, four complex values of k_z can be found, which allow nonzero solutions for $\underline{E}$. Generally, each of these four k_z values belongs to a different effective index of refraction (compare n_m in eq 2). Since two of the solutions refer to forward and two to backward propagation, the incident beam is split into the two forward beams with different propagation directions and electric polarizations (Figure 1). These "eigenpolarizations" do not, in general, coincide with any of the sample axes.[12] In the following the different eigenpolarizations, corresponding wave vectors and effective refractive indices are indexed with $_i$, where $i \in \{1, 2\}$ denotes forward propagation. In order to investigate the effects of the anisotropy on the propagation direction, in Figure 4 the propagation direction obtained by the assumption of a constant effective (and real) refractive index for both eigenpolarizations is compared with the directions obtained by numerical solutions of eq 3 for reasonable values of $\boldsymbol{n}$.

Since the eigenpolarizations are not the s and p states, we find that, due to the anisotropy of the medium, a coupling of

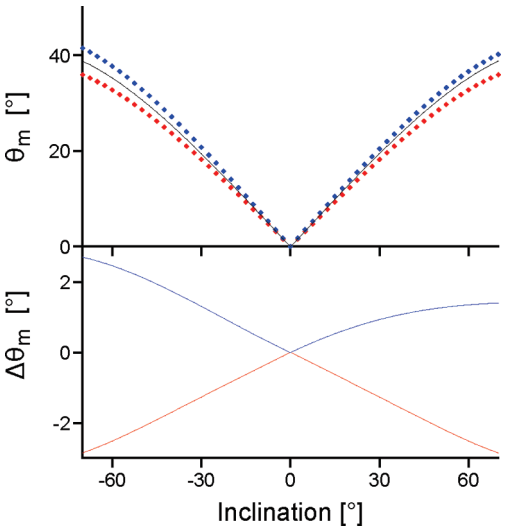

Figure 4. Comparison of inner propagation directions (expressed as θ_m, like it is defined in eq 2), The indicatrix corresponds to the sum of Re($\boldsymbol{n}$) = diag(1.4, 1.6, 1.6) and Im($\boldsymbol{n}$) = −diag(0.1,0.001,0.001), sequentially rotated about the Euler angles $\alpha_{y,z,x}$ = (15°, −15°, 33°) with respect to the y, z, and x axes. The upper plot shows the numerical solution for θ_m of eq 1 for both forward eigenpolarizations (red and blue dots) and an approximate solution according to a constant isotropic refractive index n = 1.5 (line), while the lower plot shows the differences of approximated and calculated θ_m values in the respective colors.

s and p waves appears, what means, that an incident s wave "will generate a reflected wave, that is a mixture of s and p waves".[34] Thus, finding the transmission and reflection coefficients for each beam requires the use of all four boundary conditions for electromagnetic waves besides the knowledge of all $\underline{k}_i$. This is because two transmission coefficients have to be found for each of the eigenpolarizations, since s and p waves contribute to both forward eigenpolarizations independently. If birefringence is small, the propagation directions of the forward waves are nearly identical and thus the coupling of s and p decreases. A complete analytical treatment of the problem can be found in the book by Yeh.[13]

Transition Dipole Moment Matrix. To extract molecular properties from the absorption spectra, the contribution of the molecular transition dipole moments to Im($\boldsymbol{n}$) is investigated in the following. The absorption coefficient ($\alpha(\underline{E})$) for infinitely thin films is proportional to the molecular ensemble average (denoted as $\langle\rangle$) of the scalar product $(\underline{\tilde{\mu}} \cdot \underline{E})^2$, where $\underline{\tilde{\mu}}$ is the transition dipole moment and $\underline{E}$ the electric field.[5,7] This can be converted to[35]

$$\alpha \propto \langle (\underline{\tilde{\mu}} \cdot \underline{E})^2 \rangle = \underline{E}^{\mathrm{T}} \cdot \boldsymbol{\mu} \cdot \underline{E} \qquad (4)$$

where $\boldsymbol{\mu}$ is a matrix defined by $\mu_{i,j} = \langle \underline{\tilde{\mu}}_i \, \underline{\tilde{\mu}}_j \rangle$ with $i, j \in \{x,y,z\}$. Since $\boldsymbol{\mu}$ is a symmetric matrix in the reference frame of the

sample, it can be diagonalized using an Euler rotation matrix $\boldsymbol{M}$; or in other words, it can be transformed into the reference frame of the principal axes of the absorption coefficient tensor. This means, that the diagonalized matrix $\boldsymbol{\mu}'$ (or the eigenvalues of $\boldsymbol{\mu}$) can be used to calculate a three-dimensional order parameter $\underline{S}$ of the transition moment (since it records the shape of the absorption ellipsoid), while the rotation matrix $\boldsymbol{M}$ (or the eigenvectors of $\boldsymbol{\mu}$) represent the orientation of the absorption ellipsoid.[11,15]

$$S_i = \frac{1}{2}\left(\frac{3\mu'_{i,j}}{\sum \mu'_{i,j}} - 1\right) \tag{5}$$

where the sum is performed with respect to $j \in \{x,y,z\}$. Usually $\underline{S}$ is expressed as a scalar order parameter $S_{\max}$ (denoted below simply as S), and a biaxiality parameter b, which are defined here as[15]

$$S_{\max} = \max\{S_x, S_y, S_z\} \tag{6}$$

$$b = \min_{i \neq j} \{|S_i - S_j|\} \tag{7}$$

Data Analysis

As shown in the preceding section the transmitted intensity must be analyzed in terms of inclination and polarization of the incident wave depending on the material properties (namely $\boldsymbol{n}$ and the thickness of the sample). Since finding numerical solutions of eq 3 is strongly time-consuming in a fitting algorithm, several approximations can be made recording the properties of organic polymer films in the near-infrared region.

(a) Re($\boldsymbol{n}$) $\gg$ Im($\boldsymbol{n}$); (b) The anisotropy of Re($\boldsymbol{n}$) ($=\Delta n_r/n_r \lesssim 0.06$) is small compared to the anisotropy of Im($\boldsymbol{n}$) ($=\Delta n_i/n_i \gtrsim 0.3$). The anisotropy of Re($\boldsymbol{n}$) can be measured between two crossed polarizers, and in case of weak absorption the intensity varies with the wavenumber according to[36] $\sin^2(\Delta\mathrm{Re}(\boldsymbol{n})d\pi\bar{\nu})$. (c) Interference effects can be neglected due to surface inhomogeneities. (d) Scattering will be treated as an isotropic effect. Note that the approximations (a) and (b) are proven to be true by additional measurements.

Because of the small anisotropy of Re($\boldsymbol{n}$) and the small absorption coefficient in the near-infrared range ($\propto$ Im($\boldsymbol{n}$)), $\underline{k}_1$ and $\underline{k}_2$ are almost equal and can thus be estimated from the isotropic Snell's law using an average refractive index. Here $n = n_1 = n_2 = 1.5$ is assumed, since the dependence of the transmitted intensities on inclination and polarization in nonspecific absorbing spectral regions (e.g., $\bar{\nu} \approx 5000\ \mathrm{cm}^{-1}$) indicates $n \approx 1.47$. The emerging error is small even though only one propagation direction Re(k_z) is found instead of two (compare Figure 4). The contributions of the incident electric field $\underline{E}_{in}$ to the eigenpolarizations $\underline{E}_i = E_i\underline{e}_i$, with $|\underline{e}_i| = 1$, depending on inclination and polarization are given by the reflection- and transmission coefficients at the lower sample surface. Writing them in terms of $\underline{k}_0$ and the $\underline{k}_i$, we find that for small birefringence ($\underline{k}_1 \rightarrow \underline{k}_2$) the two isotropic transmission coefficients (t_s for s polarization and t_p for p polarization as in the usual Fresnel's equations) can be used instead of the complicated four anisotropic ones. Thus, the field of the eigenpolarization i (propagating in forward direction) or the net electric field $\underline{E}_m$ at the first interface inside the medium (at $z = 0$) can be given by

$$\underline{E}_i(z = 0) = (t_s\,\underline{E}_s \cdot \underline{e}_i + t_p\,\underline{E}_p \cdot \underline{e}_i)\,\underline{e}_i \tag{8}$$

$$\underline{E}_m(z = 0) = \underline{E}_1 + \underline{E}_2 \tag{9}$$

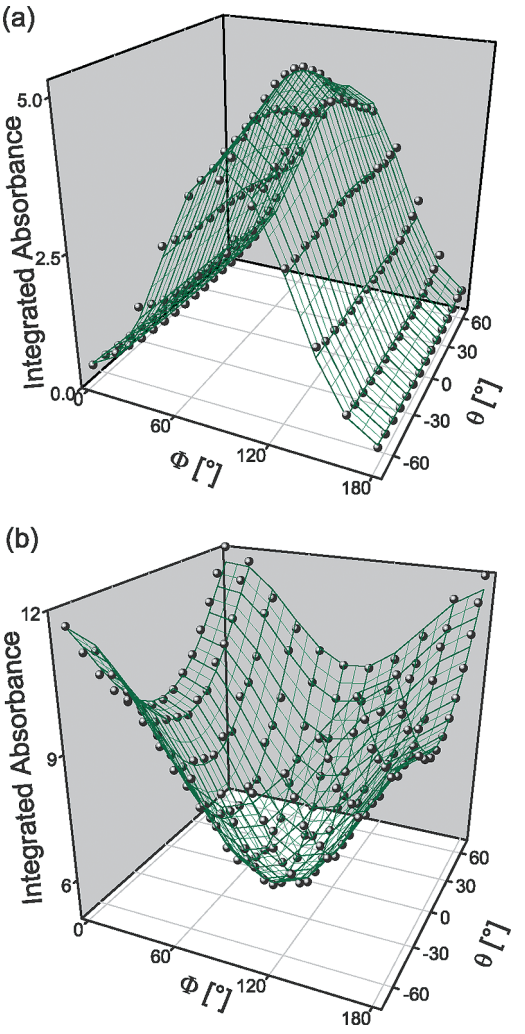

Figure 5. Measured (points) and fitted (green surface lines) integrated absorbance values of band **1** (a) and band **4** (b), After fitting the individual bands with Gaussian profiles, the area of the peaks, the integrated absorbance, can be fitted according to their dependence on θ and Φ (see eqs 2 and 8−13. Note the different symmetry of the transition dipole moments parallel (a) and perpendicular (b) to the director.

where $\underline{E}_s + \underline{E}_p + = \underline{E}_{in}$ is the decomposed incident electric field vector outside the medium. All in all, the first interface causes a rotation of the polarization direction (because $t_s \neq t_p$), a change of the propagation direction (refraction) and a decrease of the intensity (reflection). But, since $\boldsymbol{n}$ does not change significantly within the width of the absorption band, the effect of reflection at this interface can simply be treated as a rotation of the net polarization after the intensity is renormalized ($|\underline{E}_1 + \underline{E}_2| = |\underline{E}_{in}|$), what can be done by baseline subtraction.

As the polarization determines the molecular absorption coefficient (see eq 4), the respective eigenpolarizations $\underline{E}_i$ are needed as the second step. Because of the strong anisotropy of Im($\boldsymbol{n}$), again disregarding the anisotropy of Re($\boldsymbol{n}$), the directions of the eigenpolarizations $\underline{e}_i$ (as introduced above) can be estimated as the eigenvectors of Im($\boldsymbol{n}$). This means that they are equivalent to the directions corresponding to the extreme values of eq 4, which directly provides the respective absorption coefficients (α_i). So after the total electric field inside the medium $\underline{E}_m(z = 0)$ after entering the sample is calculated, it can be split into the eigenpolarizations $\underline{E}_1$ and $\underline{E}_2$ (of $\boldsymbol{\mu}$), which get independently exponentially weakened by absorption. The net electric field $\underline{E}_m(z = d)$ directly before interacting with the second

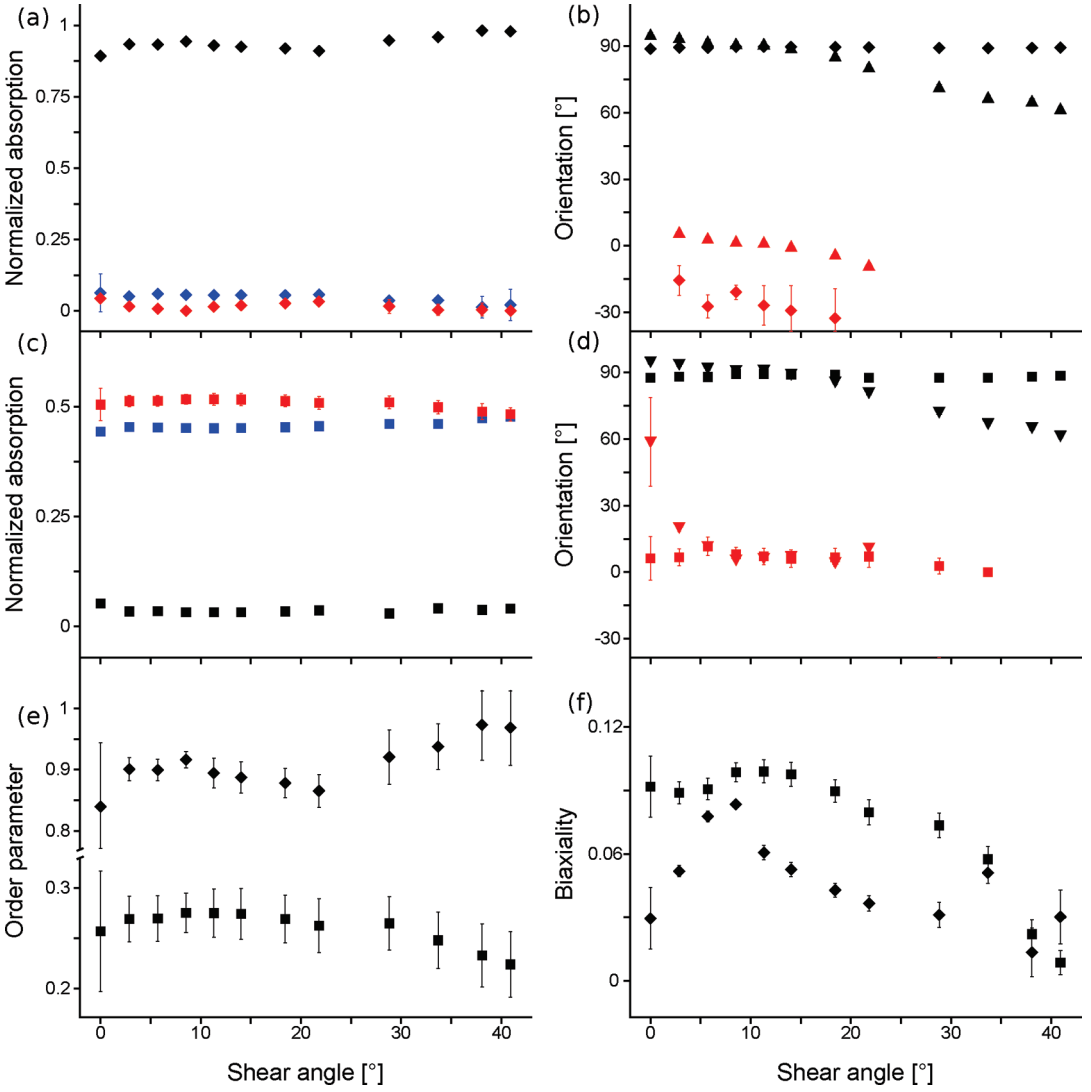

Figure 6. Fitting results of absorption band **1** and **2** (Table 1). (a and c) Length of the absorption axes of band **1** and **2**. (b and d) Spherical coordinates (θ_s, squares, and ϕ_s, triangles) of the eigenvectors of band **1** (b) and **2** (b). Black and red symbols refer to the axis of the same color in parts a and c. If the samples are nearly uniaxial, the minor and intermediate absorption axes could not be distinguished within the experimental error; thus, the orientation of the minor axis is not given. Furthermore, if $\theta_s \sim 0°$ the azimuthal angle ϕ_s is not well-defined and, hence, not shown (e) order parameter of band **1** (diamond shapes) and band **2** (squares) according to eq 5. (f) Biaxiality parameter of band **1** (diamond) and **2** (square) according to eq 7; In all cases, the error bars correspond to the 95% confidence region of the nonlinear regression and are comparable to the size of the symbols if not indicated otherwise.

interface can thus be fitted by applying attenuation to both eigenpolarizations.

$$|\underline{E}_m(z = d)|^2 = \left[\underline{E}_m(z = 0)\cdot\left(\sum_{i=1,2}\underline{e}_i \exp\left(-\frac{1}{2}\underline{e}_i^{\mathrm{T}}\cdot\boldsymbol{\mu}\cdot\underline{e}_i d_{\mathrm{eff}}\right)\right)\right]^2 \tag{10}$$

where $d_{\mathrm{eff}} = d/\cos\theta_m$ is the optical path of the wave and d the thickness of the sample. Phase effects are neglected here, since due to thickness inhomogeneities the phase differences average out.

The electric field $\underline{E}$, that passes the second interface (i.e., leaves the sample), can be composed from the amplitudes of the eigenpolarizations or from the net polarization reaching the second interface ($z = d$) in a similar way as in eq 8 and eq 9.

$$\underline{E} = \sum_{i\in\{1,2\}}\{t_s(\underline{E}_i(z = d)\cdot\underline{e}_s)\underline{e}_s + t_p(\underline{E}_i(z = d)\cdot\underline{e}_p)\underline{e}_p\} \tag{11}$$

$$= (\underline{E}_m(z = d)\cdot\underline{e}_s)t_s\underline{e}_s + (\underline{E}_m(z = d)\cdot\underline{e}_p)t_p\underline{e}_p \tag{12}$$

Since the two $\underline{E}_i(z = d)$ have undergone different absorption (according to eqs 4 and 10), the situation differs from the one at the first interface eq 8. Nevertheless, in order to correct for the intensity loss due to reflection, $\underline{E}$ is normalized again but this time with respect to the electric field that would leave a nonlossy sample.

Treating the electric field this way, background absorption as well as reflection and scattering can be split from the absorption of the transition dipole moment without disregarding the

polarization and inclination dependence of the transmission and absorption coefficients. Thus, after baseline correction the measured net absorbance A appears to be

$$A = -\log\left(\frac{\underline{E}^2}{\underline{E}_m}^2(z=0)\right) \quad (13)$$

This equation is used for fitting, an example is shown in Figure 5. Multiple reflections in the sense of interference (which could not be observed in any case) are not considered. Finally, the order parameters and the respective orientations of the transition dipole moments are calculated from $\boldsymbol{\mu}$ and their diagonal decomposition $\boldsymbol{\mu}'$ according to eq 5 and the subsequent definitions.

Since in the preceding analysis a relation is found between absorbance and molecular properties (namely $\boldsymbol{\mu}$), the last thing is to acquire the absorbance from the absorption spectra measured. To do so, the bands mentioned in Table 1 are fitted by a sum of 2 Gaussian profiles (except **2** which is fitted with a single profile) after a simple straight baseline is subtracted (an example is shown in Figure 2). The center and width of the peaks are iteratively optimized and fixed assuming a constant band shape for a given strain value independent of polarization and inclination. The resulting peak heights (or the proportional areas) are finally used as the respective absorbance values. As can be seen in Figure 2, the absorption bands **3** and **4** consist of two lines with a strong overlap, but for **3** only the line at $\bar{\nu} = 4068\ \mathrm{cm}^{-1}$ is used to extract orientation properties, since fitting the whole band as a single one yields identical results for the orientation (despite of an increased error, because the overlapping band at $\sim$4084 cm^{-1} is quite weak). Band **4** consists of two CH vibrations of same orientation with respect to the director and identical order. The sum of the corresponding absorbance values could thus be used to extract the orientation distribution.

Results and Discussion

The transition dipole moment matrix can be converted into a set of eigenvalues and eigenvectors; thus, instead of the elements of $\boldsymbol{\mu}$, its eigenvalues (normalized by their sum) are presented together with four spherical coordinate angles, that describe the orientation of the eigenvectors of the extremal eigenvalues in ordinary spherical coordinates (the inclination θ_s is measured from the surface normal corresponding to the z axis, and the azimuth ϕ_s from the x axis, compare Figure 1). Since the specificity of the IR-spectral range enables one to analyze the response of different molecular moieties independently from each other, in the following, the results obtained for all 4 bands are discussed. The absorption bands **2** to **4** are perpendicular to the director and show one minor and two major axes. Therefore, their clearly different minor axis has to be compared to the major axis of band **1**. Furthermore, it has to be stated, that if the distribution approaches uniaxiality, only one axis can be distinguished from the other and hence no minor axis orientation is given (compare e.g. $\beta > 25°$ in Figure 6b). The orientation angles of the intermediate absorption axis are omitted for clarity and the deduced quantities S and b given for comparison.

In Figure 6, the main axis of the absorption ellipsoid for absorption band **1** and their directions are presented. This band corresponds to the ester bond, which is parallel to the director. It reflects the highly anisotropic orientation distribution of the respective transition dipoles, which is already indicated by the absorbance spectra shown in Figure 2 measured at $\Phi = 0°$ and 90°. As expected a high order parameter is found even before the shear deformation is applied, because the transition dipole moment is parallel to the director. A change in the trend of the biaxiality parameter (from increasing to decreasing) can be seen

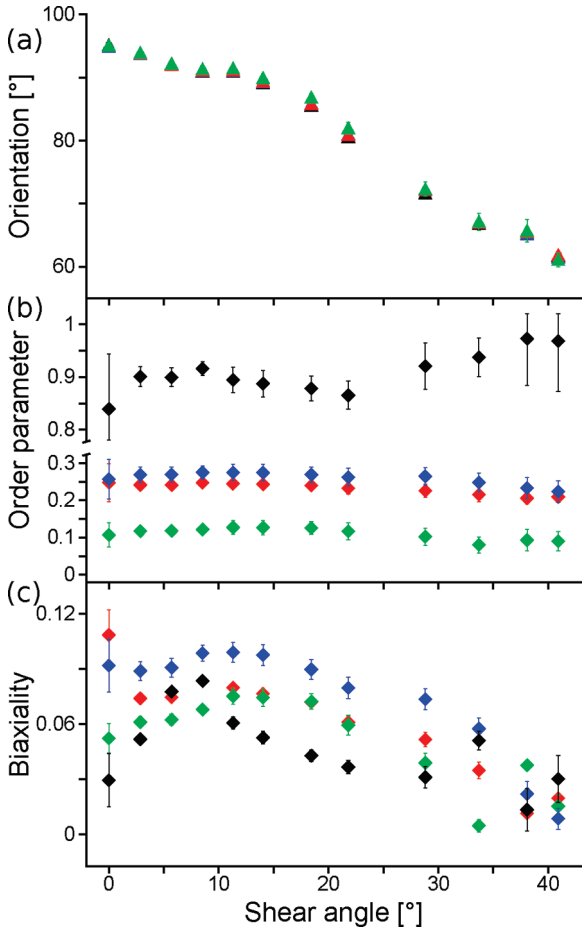

Figure 7. (a) Azimuthal angles (ϕ_s) of the main absorption axis of absorption band **1** in black are shown together with the ones of the minor axis of absorption band **2** to **4** in blue, red and green (in this sequence). (b) Order and (c) biaxiality parameters of all bands in the same colors.

at a shear angle of $\approx 10° \pm 2°$. At high shear angles a stronger reorientation of the director is observed (azimuth of the main axis), next to a continuous rotation of the minor axis into the plane of the sample. Within the experimental error no strong change of the order parameter is observed in this region, but it starts to increase at $\beta \gtrsim 25°$.

Absorption band **2** records the orientation of the mesogens in a different manner than band **1**, since the respective transition dipole moment (C═O) is perpendicular to the director, which is the reason for the lower order parameter as well (Figure 6). According to our definition, a uniaxial sample with $S = 1$ for band **1** would correspond to $S = 0.25$ for band **2**; thus, S is in accordance with the findings for band **1** as well as the decreasing biaxiality for $\beta \gtrsim 12°$ and the orientation of the minor absorption axis. The decrease of S for $\beta \gtrsim 25°$ is due to the vanishing biaxiality, while the minor absorption axis stays constant (thus $S < 0.25$).This band probes the cylindrical symmetry of the distribution and so the symmetry of the mesogen itself. It appears, that the C═O bond looses its preferential orientation along the $\underline{z}$ axis (surface normal) with shear.

This band is build up from two different aromatic C−H bonds showing unequal orientations with respect to the director. Both exhibit a nonzero component parallel to the director in opposing directions. Thus, the quadratic averaged transition dipole moment matrix exhibits an enlarged component along the director, although the main component is perpendicular to it. Hence, a lower order parameter is expected. Biaxiality (Figure 7c) and orientation (Figure 7a) of the benzene rings show similar trends

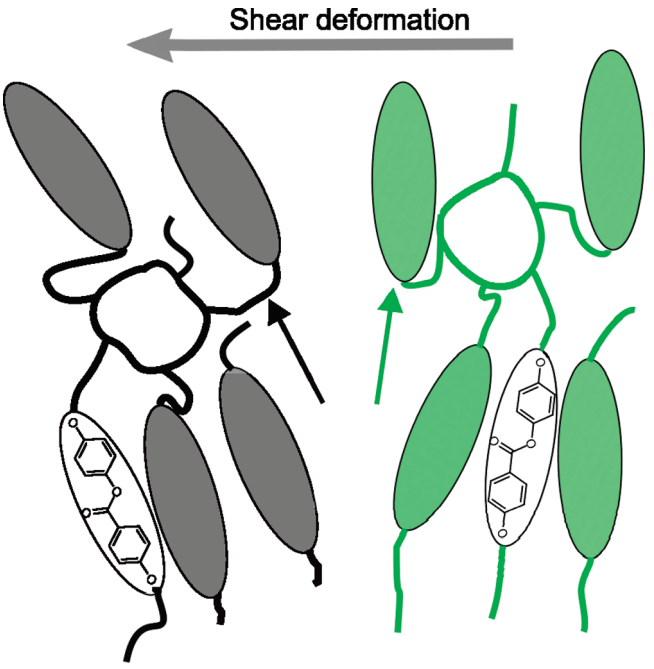

Figure 8. Sketch of the molecular arrangement before (green) and after (black) the application of the shear deformation (depicted as the gray arrow), The mesogens are indicated by the ellipsoids, the spacers and cross-linkers by the lines. The directors are shown as arrows in the respective colors.

with shearing as band **2**. Therefore, the small, explainable differences verify the accuracy of the method. Absorption band **4** corresponds to the behavior of the mesogen alkyl spacers. Because of their high flexibility they are incorporated to prevent crystallization of the mesogens, and indeed they show an even smaller order parameter than bands **2** and **3** (Figure 7). Coupling to the mesogens is quite strong, since orientation, molecular order and biaxiality display similar trends as the bands **2** and **3** even though the respective values are lower. Taking the shortness of the spacers into account the observed similarities appear naturally and, thus, verify consistency.

Finally, Figure 7a summarizes the orientations of the molecular moieties under study. It shows that all of them follow the same reorientation trend under shear consisting of 2 regimes: First for $\beta \in [0°, 14°]$ the distribution is rotated by $\sim 5°$, so that distribution and shear force are perpendicular to each other. The second regime is characterized by a nearly affine rotation of the director ($\beta \in [14°, 41°]$ and director rotation from $\sim 90°$ to $\sim 62°$).

Furthermore, the 2 regime behavior is found for biaxiality, too, where a maximum for $\beta \approx 10°$ can be found for all molecular moieties (although with different appearance). The biaxiality parameters found by Storz et al. and Severing and Saalwächter[1,2] are higher than the ones measured here (they differ by a factor of $\lesssim 2$ in a similar temperature range). This is explained by the fact that in these studies LCEs with mesogens including naphtalenes have been measured, which exhibit a stronger steric anisotropy.

The congruent rotations (Figure 8) in conjunction with the conform behavior of biaxiality and order parameters indicate a strong coupling of the different molecular moieties, probably due to their serial (chain) arrangement. Thus, it verifies the consistency of the method and confirms the idea, that entanglement, cross-linking and the inherent order govern the physical properties of such materials.

Conclusions

A new experimental approach has been presented to determine the three-dimensional orientation function (or equivalently the order parameter) of transition dipole moments in an arbitrarily oriented film. Since this method is based on IR transmission spectroscopy, the orientation distribution of different molecular moieties can be traced independently because of the specificity of vibrational absorption. Thus, any IR-translucent material can be studied in its natural state or exposed to mechanical, thermal or other excitations. Starting from Maxwell's equations the spectroscopic analysis shown takes reflection and refraction of a lossy, biaxial medium fully into account. Evaluating the transition probability then leads to the connection of optical and molecular properties (eq 4). Using only a few reasonable assumptions, that apply to most polymer films, the complex analysis can be greatly simplified. In contrast to other approaches no models concerning the orientation distribution are necessary; hence, all 6 elements of the order parameter matrix can be determined. In conclusion a comprehensive as well as detailed and consistent picture of the molecular order can be drawn using this method, revealing even the correlations between molecular moieties, as well as their response to external excitations. Furthermore, the setup offers the possibility to carry out more refined measurements, since several external parameters (temperature, humidity, ...) can be adjusted independently, while the sample can be excited in various ways (e.g., frequency dependent electric excitation, magnetic...).

In detail the response of a main-chain smectic LCE exposed to a shear deformation is measured. It turns out, that mean orientation and biaxiality reflect the serial arrangement of the moieties and show two regimes, possibly as a result of the initial director orientation exhibiting an angle of $\approx 5°$ with the sheared direction.

Acknowledgment. The financial support of the Leipzig School of Natural Sciences, BuildMoNa, is gratefully acknowledged.

References and Notes

(1) Storz, R.; Komp, A.; Hoffmann, A.; Finkelmann, H. *Macromol. Rapid Commun.* **2009**, *30*, 615–621.
(2) Severing, K.; Saalwächter, K. *Phys. Rev. Lett.* **2004**, *92*, 125501.
(3) Kang, S.; Prabhu, V. M.; Soles, C. L.; Lin, E. K.; Li Wu, W. *Macromolecules* **2009**, *42*, 5296–5302.
(4) Uribe-Patarroyo, N.; Alvarez-Herrero, A. *J. Opt. Soc. Am. B* **2009**, *26*, 1188–1195.
(5) Thulstrup, E. W.; Michl, J. *Spectroscopy with Polarized Light: Solute Alignment by Photoselection, Liquid Crystal, Polymers, and Membranes Corrected Software ed.*, 1st ed.; Wiley & Sons: New York, 1995.
(6) Sigarev, A. A.; Vij, J. K.; Hall, A. W.; Cowling, S. J.; Goodby, J. W. *Phys. Rev. E* **2007**, *76*, 051707.
(7) Griffiths, P.; Haseth, J. A. D. *Fourier Transform Infrared Spectrometry*, 2nd ed.; Wiley-Interscience: New York, 2007.
(8) Fina, L. J.; Koenig, J. L. *J. Polym. Sci., Part B: Polym. Phys.* **1986**, *24*, 2509–2524.
(9) Koenig, J. L.; Cornell, S. W.; Witenhafer, D. E. *J. Polym. Sci., Part A-2: Polym. Phys.* **1967**, *5*, 301–313.
(10) Jaworek, T.; Neher, D.; Wegner, G.; Wieringa, R. H.; Schouten, A. J. *Science* **1998**, *279*, 57–60.
(11) Jarvis, D.; Hutchinson, I.; Bower, D.; Ward, I. *Polymer* **1980**, *21*, 41–54.
(12) Yeh, P. *Surf. Sci.* **1980**, *96*, 41–53.
(13) Yeh, P. *Optical Waves in Layered Media*, illustrated ed.; John Wiley & Sons Inc: New York, 1988.
(14) Orfanidis, S. J. *Electromagn. Waves Antennas* **2008**.
(15) Warner, M.; Terentjev, E. M. *Liquid Crystal Elastomers*; Oxford Univ Press: Oxford, U.K., 2003.
(16) Donnio, B.; Wermter, H.; Finkelmann, H. *Macromolecules* **2000**, *33*, 7724–7729.
(17) Beyer, P.; Braun, L.; Zentel, R. *Macromol. Chem. Phys.* **2007**, *208*, 2439–2448.
(18) Beyer, P.; Terentjev, E. M.; Zentel, R. *Macromol. Rapid Commun.* **2007**, *28*, 1485–1490.
(19) Hiraoka, K.; Finkelmann, H. *Macromol. Rapid Commun.* **2001**, *22*, 456–460.

(20) Hiraoka, K.; Uematsu, Y.; Stein, P.; Finkelmann, H. *Macromol. Chem. Phys.* **2002**, *203*, 2205–2210.
(21) Adams, J. M.; Warner, M. *Phys. Rev. E* (*Stat., Nonlinear, Soft Matter Phys.*) **2008**, *77*, 021702–1−10.
(22) Adams, J. M.; Warner, M. *Phys. Rev. E* **2005**, *71*, 021708.
(23) Siesler, H. W. *Makromol. Chem. Macromol. Symp.* **1992**, *53*, 89–103.
(24) Siesler, H. W.; Zebger, I.; Kulinna, C.; Okretic, S.; Shilov, S.; Hoffmann, U. Segmental mobility of liquid crystals and liquid-crystalline polymers under external fields: Characterization by Fourier-Transform infrared polarization spectroscopy. In *Modern Polymer Spectroscopy*; Zerbi, G., Ed.; VCH: Weinheim, Germany, 1999; pp 67−81.
(25) Dumon, M.; Zentel, R.; Kulinna, C.; Siesler, H. W. *Liq. Cryst.* **1995**, *18*, 903–910.
(26) Heinze, P.; Finkelmann, H. *Macromolecules* **2010**, *43* 6655−6665.
(27) Komp, A.; Rühe, J.; Finkelmann, H. *Macromol. Rapid Commun.* **2005**, *26*, 813–818.
(28) Küpfer, J.; Finkelmann, H. *Makromol. Chem., Rapid Commun.* **1991**, *12*, 717–726.
(29) Pellerin, C.; Rousseau, M.; Prud'homme, R. E.; Pézolet, M. *Appl. Spectrosc.* **2002**, *56*, 17–23.
(30) Socrates, G. *Infrared and Raman Characteristic Group Frequencies. Tables and Charts*, 3rd ed.; John Wiley & Sons Ltd: 2001; pp 130−132.
(31) Workman, J.; Weyer, L. *Practical guide to interpretive near-infrared spectroscopy*; CRC Press: Boca Raton, FL, 2007; p 45.
(32) Wu, P.; Siesler, H.; Maso, F. D.; Zanier, N. *Analusis* **1998**, *26*, 61–63.
(33) Reference 30, pp 51−52.
(34) Reference 13, Chapter 9.
(35) Ikeda, R.; Chase, B.; Everall, N. J. Basics of Orientation Measurements in Infrared and Raman Spectroscopy. In *Vibrational Spectroscopy of Polymers: Principles and Practice*, 1st ed.; John Wiley & Sons: New York, 2007; pp 283−303.
(36) Reference 13, p 226.